Structure of non-global logarithms with Cambridge/Aachen clustering

K. Khelifa-Kerfa[1,2,3,4⋆]

1 Department of Physics, Faculty of Science and Technology, Relizane University, Relizane 48000, Algeria
2 Laboratory of Physics of Experimental Techniques and Applications, University of Médéa, Médéa 26000, Algeria
3 Laboratory of Thin Layers and Advanced Technologies, Relizane University, Relizane 48000, Algeria
4 Laboratory of Mathematics and Applications, University of Chlef, Chlef 02000, Algeria

⋆ kamel.khelifakerfa@univ-relizane.dz

Abstract

We determine the structure of both Abelian and non-Abelian non-global logarithms up to four loops for e^+e^- processes in perturbative QCD, where final-state jets are defined using the Cambridge-Aachen (C/A) clustering algorithm. The calculations are performed within the soft (eikonal) approximation using strong-energy ordering of the final-state partons. The resulting expressions include full colour and complete jet-radius dependence. Compared to the anti-k_t and k_t clustering algorithms, the C/A distribution minimises the impact of these non-global logarithms, making it the preferred choice among the three algorithms.

1 Introduction

Precision studies of QCD radiation at colliders increasingly rely on observables that are sensitive to restricted regions of phase space. Among these, jet substructure observables such as the jet mass constitute paradigmatic examples of so-called non-global observables. Their perturbative distributions receive leading enhancements not only from soft and collinear radiation directly associated with the hard initiating parton, but also from correlated emissions that populate disparate angular regions. The latter give rise to non-global logarithms (NGLs), which are intrinsically entangled with the pattern of colour correlations in the event and, importantly, are highly sensitive to the detailed definition of the jet employed in the analysis [1–4].

The dependence of non-global observables on the jet algorithm manifests itself through two distinct mechanisms. First, the clustering sequence of the algorithm modifies the phase space available to primary (or "global") soft–collinear radiation and generates a tower of clustering logarithms (CLs) [4–6]. Second, the algorithm alters the survival probability of correlated secondary emissions that are the source of NGLs. These two effects — the modification of primary emission contributions (CLs) and the reshaping of secondary emission patterns (NGLs) — need therefore be treated within a unified framework to achieve a controlled resummation, at least at single-logarithmic accuracy.

Over the past two decades, substantial progress has been made for specific jet definitions. For the anti-k_t algorithm [7], whose rigid cone-like clustering simplifies the geometry of final-state jets, the resummation of NGLs has been achieved through various approaches. These include, in the large-N_c limit, the Monte Carlo (MC) code of Dasgupta and Salam [1] and the Banfi–Marchesini–Smye (BMS) integro-differential equation [2], along with finite-N_c generalisations [8–11], although the latter have been implemented only for a limited set of observables. The current state-of-the-art for these resummations reaches next-to-leading NGLs accuracy, in the large-N_c limit, [12–15].

For the k_t algorithm [16,17], only MC codes in the large-N_c limit are currently available: the MC of [1], which handles both double-logarithmic (DL) and single-logarithmic (SL) observables, and the recently developed MC of [18] within the Soft-Collinear Effective Theory (SCET) framework, which currently treats only SL observables. The latter code also applies to the Cambridge-Aachen algorithm [19,20]. To date, the state-of-the-art resummation for these algorithms remains at leading NGLs (and CLs) in the large-N_c limit. No next-to-leading NGLs (or CLs) or finite-N_c resummations exist in the literature for k_t and/or C/A large logarithms. We intend to address these challenges in future work.

Despite these advances, clustering algorithms differ qualitatively in the way they order emissions and recombine particles and/or pseudo-jets. The Cambridge/Aachen algorithm, which clusters purely according to angular separation, presents particular challenges: its clustering does not respect a simple scale ordering and, hence, resummation frameworks based on an evolution in emission hardness are not readily available. Consequently, for DL-sensitive observables there is, to date, no compact evolution equation or general-purpose MC algorithm that achieves the same level of automation as for anti-k_t or k_t; progress for C/A has therefore relied on "brute-force" fixed-order calculations and tailored numerical treatments for specific observables such as the jet mass [21,22]. This absence of an ordering variable renders C/A an interesting, yet technically demanding, setup for the study of both CLs and NGLs.

To make analytical progress in this difficult setting it is customary to introduce a few ap-

proximations. Two particularly useful simplifications are the soft (eikonal) approximation, which retains only the leading soft singularities of the emission amplitudes, and the strong-energy (or strong-k_t) ordering of emissions, which reduces the combinatorial complexity of both the clustering sequence and the phase space. Within this simplified framework, one can derive semi-analytic expressions for fixed-order contributions to CLs and NGLs and, crucially, identify patterns that survive beyond these approximations. Fixed-order computations up to two loops have already exposed several robust features—the so-called boundary or "edge" effect whereby CLs and NGLs remain non-vanishing as the jet radius $R \to 0$, the dominant role of gluon-initiated channels through larger colour factors, the similarity of the gross features across different QCD environments (lepton, lepton–hadron and hadron–hadron), and the general tendency of some clustering algorithms to reduce the size of NGLs relative to anti-k_t (see, for instance, [3–6, 18, 23–30]).

In this work we extend the analyses of [22] and [31] by computing CLs and NGLs for the C/A clustering algorithm to three and four loops for the jet mass in e^+e^- annihilation into dijet processes. Working within the approximations described above, we perform the angular integrations while retaining the full colour and jet-radius (R) dependence, using high-precision numerical methods because closed-form expressions are not available. The higher-order results allow us to test exponentiation patterns and to motivate a next-to-leading-logarithmic (NLL) resummed form factor in which the global Sudakov factor multiplies exponentials that encode our fixed-order results for CLs and NGLs.

The way the C/A algorithm is structured contains, within it, the full k_t algorithm, which in turn contains the anti-k_t algorithm. This implies that the C/A algorithm explores the full set of clustering orderings: it covers the range of possible orderings and clusterings of the final-state particles, whereas k_t and anti-k_t realise only subsets, with anti-k_t covering the smallest set. Hence, just as the k_t calculations may be regarded as corrections to the anti-k_t results [1, 4, 6, 24, 31, 32], the C/A calculations represent corrections to the k_t ones [22]. We find, through three and four loops, that these corrections are generally of opposite sign to the corresponding k_t corrections. This leads to a reduction in the magnitude of both NGLs and CLs coefficients at these loop orders, and we anticipate that the trend may persist at higher orders. The jet-mass distribution appears to exhibit a pattern of exponentiation, as observed for the k_t clustering [31, 32]. Comparisons between the all-orders NLL resummations for anti-k_t and k_t — for which we use the output of the MC of [1] for NGLs and/or CLs — and our fixed-order-based exponential for C/A confirm that C/A has the strongest impact in minimising the importance of non-global logarithms. Furthermore, up to four loops the finite-N_c corrections do not appear to be significant. The dependence on the jet radius is moderate in the range $[0, 1]$.

The paper is organised as follows. In Section 2 we introduce our notation, kinematics, and the definition of the jet algorithm under study. Section 3 presents the fixed-order framework and the explicit calculations of CLs and NGLs at three, and four loops. We note that the two-loop results have been previously computed in the literature (see, e.g., [4, 6, 21, 23, 24, 27, 33]). In Section 4 we compare our fixed-order-based exponentiation with all-orders Monte Carlo resummations for the anti-k_t and k_t algorithms, and discuss the impact of NGLs and CLs arising from the C/A algorithm. Section 5 summarises our conclusions and outlines potential directions for future work.

2 Observable and jet algorithm definitions

The majority of this section follows the approach detailed in Ref. [31]. We shall therefore only report the essential ideas and notation herein to ensure the paper's self-consistency. As

stated in the introduction, we consider the invariant squared mass of the two leading jets in e^+e^- annihilation processes in the threshold limit, which serves as an example to illustrate our main points. In particular, we consider the partonic process:

$$e^+ + e^- \to q(p_a) + \bar{q}(p_b) + g_1(k_1) + \cdots + g_n(k_n), \tag{1}$$

where the four-momenta of the final-state partons are defined by

$$p_a = \tfrac{Q}{2}(1,0,0,1), \qquad p_b = \tfrac{Q}{2}(1,0,0,-1), \qquad k_i = \omega_i(1, s_i \cos\phi_i, s_i \sin\phi_i, c_i), \tag{2}$$

with $c_i \equiv \cos\theta_i$ and $s_i \equiv \sin\theta_i$. Here, Q is the hard scale of the process, ω_i is the energy of the ith soft gluon, and θ_i and ϕ_i are its polar and azimuthal angles, respectively. Our calculations are performed within the eikonal (soft) approximation, assuming massless partons, neglecting recoil effects, and imposing a strong ordering of the gluon energies: $Q \gg \omega_1 \gg \omega_2 \gg \cdots \gg \omega_n$. Whilst these approximations significantly simplify the calculations, they only guarantee single-logarithmic accuracy. As this paper presents a pioneering study of the C/A jet algorithm beyond two loops, it is sufficient to work at this level of accuracy, particularly given the substantial complexity involved. Future work will extend this to higher-order logarithmic contributions.

The observable we consider in this paper is the normalised invariant mass squared of the final-state dijets:

$$\varrho = \varrho_{\text{R}} + \varrho_{\text{L}}, \tag{3}$$

where $\varrho_{\text{R(L)}}$ denotes the normalised invariant mass squared of the right (left) jet, initiated by the final-state quark (antiquark). Given the analogous expressions for both jets, we present only the explicit formula for ϱ_{R}. To this end, we have [31]

$$\varrho_{\text{R}} = \frac{4\,m_{\text{R}}^2}{Q^2} = \frac{4}{Q^2} \left(p_a + \sum_{i \in j_{\text{R}}} k_i \right)^2 = \sum_{i \in j_{\text{R}}} \varrho_{\text{R},i} + \mathcal{O}\left(\frac{\omega^2}{Q^2} \right),$$
$$\varrho_{\text{R},i} = \frac{8\,(p_a \cdot k_i)}{Q^2} = 2x_i(1 - c_i), \tag{4}$$

where we have defined the energy fraction of the ith gluon as $x_i \equiv 2\omega_i/Q$. The sum in the first line runs over all gluon emissions that are clustered, by the C/A algorithm, into the right jet j_{R}. For the left jet, j_{R} is replaced by j_{L}. Terms of order $(\omega/Q)^2$ and higher are neglected, consistent with the soft approximation.

2.1 C/A jet algorithm

The C/A jet algorithm was first introduced in Refs. [19,20]. It can be considered a member of the generalised k_t family of algorithms defined in Ref. [34], which comprises a set of sequential recombination jet algorithms parametrised by a continuous variable p. For e^+e^- processes, these algorithms proceed as follows:

1. For an initial list of final-state particles, define the following two distance measures for each pair (i, j):

$$d_{ij} = \min\left(E_i^{2p}, E_j^{2p} \right) \frac{1 - \cos\theta_{ij}}{1 - c_R}, \qquad d_{iB} = E_i^{2p}, \tag{5}$$

where $c_R = \cos R$ with R the jet-radius parameter, E_i is the energy of the ith particle, and $\cos\theta_{ij} = c_i c_j + s_i s_j \cos\phi_{ij}$ with $\phi_{ij} \equiv \phi_i - \phi_j$. The quantity d_{iB} represents the distance of particle i to the beam direction.

2. Find the smallest distance amongst all d_{ij} and d_{iB}. If the minimum is a d_{ij}, then particles i and j are merged into a single pseudo-jet, with a momentum given by the sum of their constituent momenta (the E-scheme). If the minimum is a d_{iB}, then particle i is identified as a final jet and removed from the list of particles.

3. Repeat steps 1 and 2 until no particles remain.

For the C/A algorithm, the parameter $p = 0$. Consequently, the distance d_{ij} is purely geometrical and $d_{iB} = 1$. A sufficient condition for d_{ij} to be the smallest distance—and hence for the particle pair (i, j) to be clustered—is simply

$$1 - \cos \theta_{ij} < 1 - c_R. \tag{6}$$

In the small-angle limit, this condition reduces to $\theta_{ij} < R$. That is, two particles are merged if they lie within a circle of radius R in the (θ, ϕ) plane.

A pivotal aspect where the C/A algorithm differs from the anti-k_t and k_t algorithms in our analytical calculations is that we must consider all possible orderings of the distances d_{ij} at a given loop order. For the anti-k_t and k_t algorithms, the strong energy ordering of the soft gluons automatically induces a unique hierarchy of the distances d_{ij}. The unique clustering sequence for the k_t algorithm is, in fact, just one of the many possible sequences for the C/A algorithm. Therefore, the C/A distribution inherently contains the k_t result. Furthermore, since the k_t distribution itself contains the anti-k_t result [4, 21, 24, 31], the C/A distribution encompasses both the anti-k_t and k_t results, constituting a much more general distribution.

For each possible ordering of the C/A distances d_{ij}, we apply the remaining steps of the algorithm to every gluon configuration at a given loop order (as will be detailed later). This procedure leads to a reshuffling of soft gluons in and out of the measured jets. We retain only those configurations where a mis-cancellation occurs between real emissions and virtual corrections. These are the configurations that give rise to the large logarithmic terms. Given the two types of gluon emissions—primary (Abelian) and secondary correlated (non-Abelian)— two distinct types of large logarithms arise, as noted in the introduction: (Abelian) clustering logarithms (CLs) and (non-Abelian) non-global logarithms (NGLs).

2.2 Observable distribution

Following our previous work [31], we consider the integrated cross-section for the normalised dijet mass squared, $\Sigma(\rho)$, defined by:

$$\Sigma(\rho) = \int \frac{1}{\sigma_0} \frac{\mathrm{d}\sigma}{\mathrm{d}\varrho} \Theta \left[\rho - \varrho \left(k_1, k_2, \ldots, k_n \right) \right] \Xi \left(k_1, k_2, \ldots, k_n \right) \mathrm{d}\varrho, \tag{7}$$

where ρ is a veto on the (normalised) dijet mass squared $\varrho(k_1, k_2, \ldots, k_n)$ defined in eq. (3), and σ_0 is the corresponding Born cross-section. The function $\Xi(k_1, k_2, \ldots, k_n)$ represents the C/A clustering function, which constrains the integration to the regions of phase space corresponding to mis-cancellations between real emissions and virtual corrections that contribute to the dijet mass.

The perturbative expansion of the jet-mass cross-section may be written as:

$$\Sigma(\rho) = \Sigma_1(\rho) + \Sigma_2(\rho) + \cdots, \tag{8}$$

where the mth-order contribution is given by:

$$\Sigma_m(\rho) = \sum_X \int_{x_1 > x_2 > \cdots > x_m} \prod_{i=1}^m \mathrm{d}\Phi_i \, \hat{\mathcal{U}}_m \mathcal{W}_{12\ldots m}^X \, \Xi_m \left(k_1, k_2, \ldots, k_m \right). \tag{9}$$

The various terms are defined as follows:

- The sum is over all possible gluonic configurations x. Each gluon can be either real (R) or virtual (V), and x represents the set of all possible real/virtual assignments for the m gluons at a given order. For instance, at one loop, x may be R or V, and at two loops, it may be RR, RV, VR, or VV. The number of distinct configurations at mth order in perturbation theory is 2^m.

- The integration is performed under the constraint of strong-energy ordering of the soft gluons, represented by $x_1 > x_2 > \cdots > x_m$. This constraint may sometimes be relaxed, in which case a factor of $m!$ is included to avoid double-counting identical phase-space regions.

- The phase-space element for the emission of the ith gluon is given by:

$$\mathrm{d}\Phi_i = \bar{\alpha}_s \frac{\mathrm{d}x_i}{x_i} \mathrm{d}c_i \frac{\mathrm{d}\phi_i}{2\pi}, \tag{10}$$

  with $\bar{\alpha}_s = \alpha_s/\pi$.

- The measurement operator at order m, $\hat{\mathcal{U}}_m$, first introduced in Ref. [35], selects gluonic configurations that contribute to the dijet mass observable with a value less than ρ. Configurations that do not contribute to the dijet mass, or that yield a value larger than ρ, are excluded from the integrated cross-section. It can be shown that this operator factorises into a product of single-gluon measurement operators [31, 35–37]:

$$\hat{\mathcal{U}}_m = \sum_i \hat{u}_i, \qquad \hat{u}_i = \Theta_i^{\mathrm{V}} + \Theta_i^{\mathrm{R}}\left[\Theta_i^{\mathrm{out}} + \Theta_i^{\mathrm{in}}\Theta(\rho - \varrho_i)\right] = 1 - \Theta_i^{\mathrm{R}}\Theta_i^{\mathrm{in}}\Theta_i^{\rho}. \tag{11}$$

  Here, the step functions $\Theta_i^{\mathrm{R(V)}}$ equal 1 if gluon i is real (virtual) and 0 otherwise; $\Theta_i^{\mathrm{in(out)}}$ equals 1 if gluon i is inside (outside) either jet and 0 otherwise; and Θ_i^{ρ} equals 1 if $\varrho_i > \rho$ and 0 otherwise. The complementarity relations $\Theta_i^{\mathrm{R}} + \Theta_i^{\mathrm{V}} = 1$ and $\Theta_i^{\mathrm{in}} + \Theta_i^{\mathrm{out}} = 1$ hold. The final equality in (11) follows from these relations.

- The eikonal amplitude squared for the emission of m soft, energy-ordered gluons in configuration x, normalised to the Born cross-section, is denoted $\mathcal{W}_{12\ldots m}^x$. Detailed expressions for e^+e^- processes are provided in Ref. [38, 39] (and for hadronic processes with three hard legs in Ref. [40]), with explicit results given up to four loops.

- The C/A clustering function at mth order, $\Xi_m(k_1, k_2, \ldots, k_m)$, discussed in the previous section, encapsulates the clustering constraints imposed by the C/A algorithm on a specific configuration x for it to contribute to the dijet mass.

In the next section, we present detailed calculations of the third- and fourth-order terms in the perturbative expansion (8). First, however, we recapitulate the one- and two-loop results, which are identical to the k_t algorithm case presented in Ref. [31].

3 Fixed-order calculations

From the definition of the generalised k_t algorithm presented in the previous section, it is straightforward to see that all members of this family are identical at one-loop order. At two-loop order, the k_t ($p = 1$) and C/A ($p = 0$) algorithms begin to differ from the anti-k_t ($p = -1$), while remaining identical to each other. This occurs because, at two loops, we have the emission of two soft gluons k_1 and k_2, and the possible distance measures are simply d_{1B}, d_{2B},
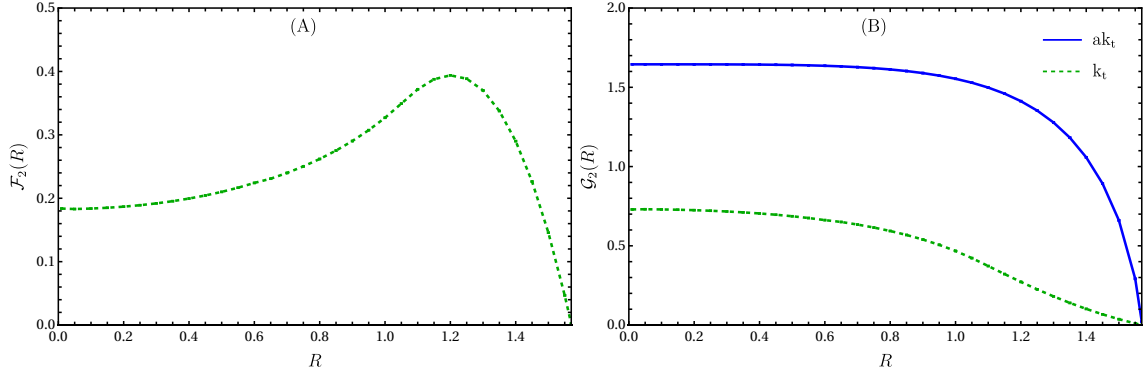
Figure 1: The two-loop CLs and NGLs coefficients for the k_t jet algorithm (from Ref. [31]).

and d_{12}. Gluonic configurations that lead to the appearance of CLs and NGLs typically correspond to the clustering of the two soft gluons first. This requires that d_{12} be the smallest distance [4, 21, 24, 31]. In analytical calculations, each gluon is typically assigned an initial position, either inside or outside the measured jets. The clustering of the two gluons means that the harder gluon k_1 pulls the softer gluon k_2 into its region, resulting in both gluons being either inside or outside the jets, depending on the initial location of k_1. For both the k_t and C/A algorithms, this is the only possible ordering of the distance measures that gives rise to large logarithms not present in the anti-k_t case. The difference between the two algorithms emerges at three loops, as will be discussed later.

The one- and two-loop results are given by [24, 31]:

$$\Sigma_1(\rho) = -C_F \bar{\alpha}_s \left[L^2 - \left(\frac{3}{2} - 2\ln\frac{1-c_R}{1+c_R} \right) L \right], \tag{12a}$$

where $L = \ln(1/\rho)$, and

$$\Sigma_2(\rho) = \frac{1}{2!} (\Sigma_1)^2 + \Sigma_{2,cl}^{k_t,C/A} + \Sigma_{2,ng}^{k_t,C/A}, \tag{12b}$$

with the CLs and NGLs distributions given by:

$$\Sigma_{2,cl}^{k_t,C/A}(\rho) = 2\bar{\alpha}_s^2 \frac{L^2}{2!} C_F^2 \mathcal{F}_2(R), \tag{12c}$$

$$\Sigma_{2,ng}^{k_t,C/A}(\rho) = -2\bar{\alpha}_s^2 \frac{L^2}{2!} C_F C_A \mathcal{G}_2(R), \tag{12d}$$

where $\mathcal{F}_2(R)$ and $\mathcal{G}_2(R)$ are the two-loop CLs and NGLs coefficients, respectively, plotted in Fig. 1. The colour factors are $C_F = (N_c^2 - 1)/2N_c$ and $C_A = N_c$, where N_c denotes the number of colours. Recall that correlated emissions from gluons inside the quark jet that end up in the antiquark jet, or vice versa, yield non-global logarithms that are subleading, as shown in Refs. [6, 24].

3.1 Three loops

This is the first order at which the C/A and k_t jet algorithms begin to differ. For the emission of three soft, strong energy-ordered gluons, there are six distance measures to compare: $d_{1q}, d_{2q}, d_{3q}, d_{12}, d_{13}$, and d_{23}. We consider only one jet (the quark jet), though a similar treatment applies to the antiquark jet. Table 1 details all configurations before and after applying

Δ_{12q}	Δ_{13q}	Δ_{23q}	Orderings	1_{in}	2_{in}	3_{in}	$(1,2)_{\text{in}}$	$(1,3)_{\text{in}}$	$(2,3)_{\text{in}}$	$(1,2,3)_{\text{in}}$
0	0	0	-	0	0	C	0	C	C	C
1	0	0	-	0	0	C	0	C	C	C
0	1	0	-	0	0	C	0	C	C	C
0	0	1	-	0	0	C	0	C	C	C
1	1	0	-	0	0	C	0	C	C	C
1	0	1	$d_{12} < d_{23}$	0	0	C	0	C	C	C
1	0	1	$d_{23} < d_{12}$	0	0	C	0	C	C	C
0	1	1	-	0	0	C	0	C	C	C
1	1	1	-	0	0	C	0	C	C	C

Table 1: Clustering patterns for the C/A algorithm at three loops.

the C/A algorithm, where $\Delta_{ijq} \equiv \Theta\left(d_{jq} - d_{ij}\right)$ with $i < j$, and the letter C indicates a mis-cancellation between real emissions and their corresponding virtual corrections. Such mis-cancellations are the source of large logarithmic terms—either non-global logarithms, clustering logarithms, or both.

A gluon k_i is considered inside the measured jet (denoted i_{in} in Table 1) if it satisfies the clustering condition (6); otherwise, it is outside the jet and not explicitly shown. For example, in the fifth column, 1_{in} indicates that only gluon k_1 is initially inside the jet (prior to C/A clustering), while k_2 and k_3 are outside. Similarly, in the penultimate column, only k_2 and k_3 are initially inside, whilst k_1 is outside. The remaining columns follow the same labelling convention.

Note that $\Delta_{ijq} = 1$ implies $d_{jq} > d_{ij}$, meaning gluons k_i and k_j are clustered first by the C/A algorithm. Since k_j is softer than k_i, it is pulled toward the harder gluon's position—either into or out of the measured jet, depending on k_i's initial location. This "dragging" mechanism spoils the complete cancellation between real and virtual contributions to the jet mass observable, thereby generating large logarithms. Conversely, $\Delta_{ijq} = 0$ implies $d_{jq} < d_{ij}$, so gluon k_j remains part of the measured (quark) jet.

The "Orderings" column lists possible hierarchies of the distance measures d_{ij} for which the corresponding $\Delta_{ijq} = 1$. For instance, in rows 6 and 7, $\Delta_{12q} = \Delta_{23q} = 1$ indicates that the two smallest distances are d_{12} and d_{23}. As the C/A algorithm requires identifying the absolute minimum, we consider both orderings $d_{12} < d_{23}$ and $d_{23} < d_{12}$ in analytical calculations. When different orderings yield distinct outcomes, both are explicitly shown; a dash (—) indicates that the ordering does not affect the final clustering result, as in the last row where all $\Delta_{ijq} = 1$.

As an illustrative example, consider the scenarios in rows 6 and 7. Table 2 shows the outcome of the C/A algorithm for all gluonic configurations at three loops, specifically for the ordering $d_{12} < d_{23}$. Here, "RRR" denotes all three gluons as real, "RRV" indicates only gluon 3 is virtual, and so forth. We reiterate that a gluon contributes to the measured jet mass only if it is real and clustered into the jet by the algorithm.

For the scenario where only gluon 1 is initially inside the measured jet (1_{in}) and all gluons are real, the condition $d_{12} < d_{23}$ combined with strong-energy ordering means that gluon 1 pulls gluon 2 into the jet. They form a subjet with four-momentum approximately equal to that of the harder gluon 1. In the second clustering step, only gluons 1 and 3 remain. Since $\Delta_{13q} = 0$ (row 6 of Table 1), these gluons cannot cluster, and the algorithm terminates. The final outcome is gluons 1 and 2 inside the measured jet and gluon 3 outside. The same outcome occurs for the RRV configuration, but since it involves one virtual gluon (gluon 3), its emission amplitude equals minus that of RRR in the eikonal limit. Consequently, the RRR and RRV configurations cancel exactly. Following the same procedure, we find that although

	RRR	RRV	RVR	VRR	RVV	VRV	VVR	VVV	sum
1_{in}	$(1,2)_{in}$	$(1,2)_{in}$	$(1)_{in}$	none	$(1)_{in}$	none	none	none	0
2_{in}	none	none	none	$(2,3)_{in}$	none	$(2)_{in}$	none	none	0
3_{in}	$(3)_{in}$	none	$(3)_{in}$	none	none	none	$(3)_{in}$	none	C
$(1,2)_{in}$	$(1,2)_{in}$	$(1,2)_{in}$	$(1)_{in}$	$(2,3)_{in}$	$(1)_{in}$	$(2)_{in}$	none	none	0
$(1,3)_{in}$	$(1,2,3)_{in}$	$(1,2)_{in}$	$(1,3)_{in}$	none	$(1)_{in}$	none	$(3)_{in}$	none	C
$(2,3)_{in}$	$(3)_{in}$	none	$(3)_{in}$	$(2,3)_{in}$	none	$(2)_{in}$	$(3)_{in}$	none	C
$(1,2,3)_{in}$	$(1,2,3)_{in}$	$(1,2)_{in}$	$(1,3)_{in}$	$(2,3)_{in}$	$(1)_{in}$	$(2)_{in}$	$(3)_{in}$	none	C

Table 2: Outcome of C/A algorithm for various gluon configurations at three loops, for the specific case $d_{12} < d_{23}$.

the RVR and RVV configurations contribute to the jet mass, they also cancel. The remaining configurations yield no contribution, resulting in a total sum of zero.

The 2_{in} case follows a similar analysis. We note that the VRR and VRV configurations cancel in the strong-energy ordering regime.

For the 3_{in} case in the RRR configuration, gluons 1 and 2 are outside the measured jet and merge into a subjet aligned with the four-momentum of the harder gluon 1. Since $\Delta_{13q} = 0$, gluon 3 is not pulled out of the jet by gluon 1 and thus contributes to the jet mass. This contribution cancels against the RVR configuration (where gluon 2 is virtual). However, the VVR configuration yields a similar contribution to RRR but lacks a counterterm to cancel against. This mismatch between real and virtual diagrams results in a non-zero total contribution, generating both NGLs and CLs.

For the $(1,2)_{in}$ case, one may verify that the sum is zero. Note that in the VRR configuration, since gluon 1 is virtual, the smallest distance is d_{23}, so gluon 3 is pulled into the jet by the harder gluon 2.

For the $(1,3)_{in}$ case, the RRR and RRV configurations cancel due to strong-energy ordering, as do RVR and RVV. In the VRR configuration, gluon 1 is virtual and unaffected by the algorithm, so the smallest distance becomes d_{23}. The harder gluon 2 then pulls the softer gluon 3 out of the jet, yielding no contribution. Consequently, the VVR configuration has no counterpart to cancel against and contributes to the jet mass, resulting in a non-zero total.

For the $(2,3)_{in}$ case, the VVR configuration lacks a counterterm and contributes to the jet mass. Finally, when all three gluons are inside the jet $(1,2,3)_{in}$, all configurations cancel except VVR, which causes a real-virtual mismatch and yields a non-zero total.

Table 3 shows the outcomes for the ordering $d_{23} < d_{12}$ (row 7). This ordering occurs in the k_t jet algorithm, where the smallest distance is between the two softest gluons (2 and 3). Although this scenario is already included in k_t calculations [31], we analyse Table 3 in detail as it was not explicitly studied in that reference.

For the case where only gluon 1 is inside the jet (1_{in}) in the RRR configuration, gluons 2 and 3 cluster first, forming a subjet aligned with gluon 2's four-momentum. This subjet then clusters with gluon 1, bringing all three gluons into the jet. This contribution cancels against RRV due to strong-energy ordering. In the RVR configuration, gluons 1 and 3 cannot cluster ($\Delta_{13q} = 0$), so only gluon 1 remains in the jet. The same outcome occurs for RVV but with opposite sign, leading to cancellation. The total sum is zero. The (2_{in}) case is trivial and also gives zero.

For the (3_{in}) case, only the RVR and VVR configurations contribute to the jet mass. Their eikonal amplitudes differ, so they do not cancel in general, particularly for NGLs. However, for CLs (from the primary emission part of the eikonal amplitudes), they do cancel [21,31,32,38]. Since our formalism includes both NGLs and CLs, we retain this as a real-virtual mismatch,

	RRR	RRV	RVR	VRR	RVV	VRV	VVR	VVV	sum
1_{in}	$(1,2,3)_{\text{in}}$	$(1,2)_{\text{in}}$	$(1)_{\text{in}}$	none	$(1)_{\text{in}}$	none	none	none	0
2_{in}	none	none	none	$(2,3)_{\text{in}}$	none	$(2)_{\text{in}}$	none	none	0
3_{in}	none	none	$(3)_{\text{in}}$	none	none	none	$(3)_{\text{in}}$	none	C
$(1,2)_{\text{in}}$	$(1,2,3)_{\text{in}}$	$(1,2)_{\text{in}}$	$(1)_{\text{in}}$	$(2,3)_{\text{in}}$	$(1)_{\text{in}}$	$(2)_{\text{in}}$	none	none	0
$(1,3)_{\text{in}}$	$(1,2,3)_{\text{in}}$	$(1,2)_{\text{in}}$	$(1)_{\text{in}}$	none	$(1)_{\text{in}}$	none	$(3)_{\text{in}}$	none	C
$(2,3)_{\text{in}}$	none	none	$(3)_{\text{in}}$	$(2,3)_{\text{in}}$	none	$(2)_{\text{in}}$	$(3)_{\text{in}}$	none	C
$(1,2,3)_{\text{in}}$	$(1,2,3)_{\text{in}}$	$(1,2)_{\text{in}}$	$(1,3)_{\text{in}}$	$(2,3)_{\text{in}}$	$(1)_{\text{in}}$	$(2)_{\text{in}}$	$(3)_{\text{in}}$	none	C

Table 3: Outcome of C/A algorithm for various gluon configurations at three loops, for the specific case $d_{23} < d_{12}$.

resulting in a non-zero total.

The $(1,2)_{\text{in}}$ case leads to complete cancellation among real and virtual diagrams, yielding no contribution. For $(1,3)_{\text{in}}$ in the RRR configuration, gluon 2 pulls the softest gluon 3 out of the jet during the first clustering. The resulting subjet (aligned with gluon 2) is then pulled into the jet by gluon 1. This contribution cancels against RRV. The RVR and RVV contributions cancel, as do VRR and VRV, leaving only VVR uncancelled and yielding a non-zero total.

For the $(2,3)_{\text{in}}$ case, VRR and VRV cancel under strong-energy ordering, but RVR and VVR do not due to different eikonal amplitudes, creating a real-virtual mismatch that contributes to the jet mass. Finally, for $(1,2,3)_{\text{in}}$, all configurations cancel except VVR, which contributes to the jet mass.

The following points are worth noting:

- Cases leading to real-virtual mismatches (and thus large logarithms) are those where the *softest* gluon is initially inside the jet region.

- The mis-cancellation can arise from a single diagram or multiple diagrams with different eikonal emission amplitudes.

- The difference between C/A and k_t clustering arises when the two harder gluons cluster first, while the hardest and softest gluons cannot cluster. This prevents the softest gluon from being dragged in or out, unlike in k_t where the softest gluon is always affected.

Summing over all gluon configurations in Table 1 for the emission of three soft, energy-ordered gluons, we find that

$$\sum_X \hat{\mathcal{U}}_3 \, \mathcal{W}_{123}^{X,\text{C/A}} = \sum_X \hat{\mathcal{U}}_3 \, \mathcal{W}_{123}^{X,k_t} - \Theta_1^{\text{out}} \Theta_3^{\text{in}} \Theta_3^\rho \Omega_{12} \Omega_{23} \bar{\Omega}_{13} \Delta_{123} \left[\mathcal{W}_{123}^{\text{VVR}} + \mathcal{W}_{123}^{\text{RVR}} + \mathcal{W}_{123}^{\text{RRR}} \right], \quad (13)$$

where the first term corresponds to the k_t jet clustering result, already computed in Ref. [31] (eq. (52)). The constraint Ω_{ij} is defined as the Heaviside function $\Theta(d_{jB} - d_{ij})$. When $\Omega_{ij} = 1$, the parton pair (ij) is closer to each other than parton j is to the beam direction.

As explained earlier, the effect of the C/A algorithm on the jet mass distribution incorporates that of the k_t algorithm, since it involves all possible orderings—only a subset of which are covered by the k_t algorithm. Substituting into eq. (9) yields:

$$\Sigma_3^{\text{C/A}}(\rho) = \Sigma_3^{k_t}(\rho) + \widetilde{\Sigma}_3^{\text{C/A}}(\rho),$$
$$= \frac{1}{3}(\Sigma_1)^3 + \Sigma_1 \times \left(\Sigma_{2,\text{cl}}^{\text{C/A}} + \Sigma_{2,\text{ng}}^{\text{C/A}} \right) + \Sigma_{3,\text{cl}}^{\text{C/A}} + \Sigma_{3,\text{ng}}^{\text{C/A}}, \quad (14)$$
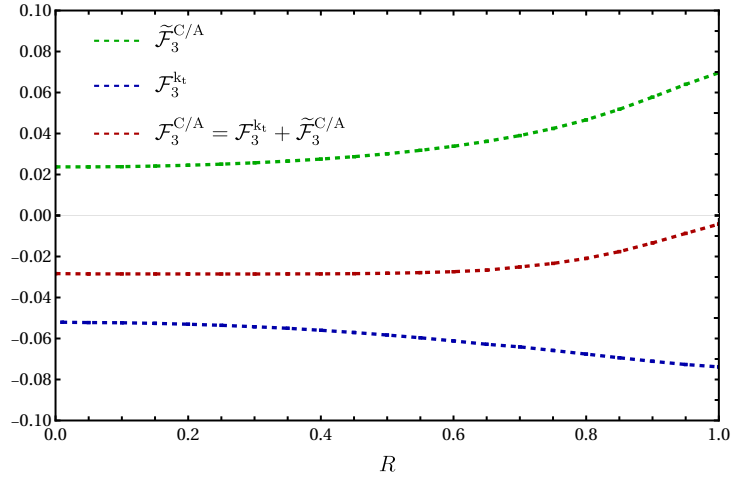
Figure 2: The three-loop CLs coefficient for the C/A and k_t jet algorithms.

where Σ_1, $\Sigma_{2,\text{cl}}^{\text{C/A}}$, and $\Sigma_{2,\text{ng}}^{\text{C/A}}$ denote the one-loop (12a), two-loop CLs (12c), and two-loop NGLs (12d) contributions to the jet mass fraction, respectively. The new three-loop CLs and NGLs contributions are given by the final two terms:

$$\Sigma_{3,\text{cl}}^{\text{C/A}}(\rho) = \Sigma_{3,\text{cl}}^{k_t}(\rho) + \widetilde{\Sigma}_{3,\text{cl}}^{\text{C/A}}(\rho) = -2\bar{\alpha}_s^3 \frac{L^3}{3!} C_F^3 \left[\mathcal{F}_3^{k_t} + \widetilde{\mathcal{F}}_3^{\text{C/A}} \right], \tag{15}$$

$$\Sigma_{3,\text{ng}}^{\text{C/A}}(\rho) = \Sigma_{3,\text{ng}}^{k_t}(\rho) + \widetilde{\Sigma}_{3,\text{ng}}^{\text{C/A}}(\rho) = +2\bar{\alpha}_s^3 \frac{L^3}{3!} \left[C_F^2 C_A \left(\mathcal{G}_{3,a}^{k_t} + \widetilde{\mathcal{G}}_{3,a}^{\text{C/A}} \right) + C_F C_A^2 \left(\mathcal{G}_{3,b}^{k_t} + \widetilde{\mathcal{G}}_{3,b}^{\text{C/A}} \right) \right], \tag{16}$$

The k_t results for both CLs and NGLs have been presented in Ref. [31] (eqs. (55), (56), and (57), and Fig. 4). The new C/A clustering corrections are given by:

$$\widetilde{\mathcal{F}}_3^{\text{C/A}}(R) = \int_{1_{\text{out}}} \int_{3_{\text{in}}} \Omega_{12}\Omega_{23}\bar{\Omega}_{13}\,\Theta\left(d_{23} - d_{12}\right) w_{ab}^1 w_{ab}^2 w_{ab}^3, \tag{17}$$

for the CLs coefficient, and

$$\widetilde{\mathcal{G}}_{3,a}^{\text{C/A}}(R) = -\frac{1}{2} \int_{1_{\text{out}}} \int_{3_{\text{in}}} \Omega_{12}\Omega_{23}\bar{\Omega}_{13}\Theta\left(d_{23} - d_{12}\right) w_{ab}^1 \mathcal{A}_{ab}^{23}, \tag{18a}$$

$$\widetilde{\mathcal{G}}_{3,b}^{\text{C/A}}(R) = -\frac{1}{4} \int_{1_{\text{out}}} \int_{3_{\text{in}}} \Omega_{12}\Omega_{23}\bar{\Omega}_{13}\Theta\left(d_{23} - d_{12}\right) \mathcal{B}_{ab}^{123}, \tag{18b}$$

for the NGLs coefficients.

In Fig. 2, we plot $\mathcal{F}_3^{k_t}$, $\widetilde{\mathcal{F}}_3^{\text{C/A}}$, and their sum $\mathcal{F}_3^{\text{C/A}} = \widetilde{\mathcal{F}}_3^{\text{C/A}} + \mathcal{F}_3^{k_t}$, which represents the CLs coefficient for the C/A algorithm at three loops. In the limit $R \to 0$, we obtain $\mathcal{F}_3^{\text{C/A}}(0) = -0.028$, confirming our previous calculations [21]. The persistence of CLs even as the jet radius shrinks to zero is a phenomenon known as the *edge* or *boundary* effect, previously observed for both CLs and NGLs in anti-k_t and k_t algorithms (see, e.g., Refs. [6,24,31,41]). Fig. 2 clearly shows that this behaviour also occurs for the C/A algorithm. Moreover, the small-R limit of the CLs coefficient for our jet mass observable is both much smaller and of opposite sign compared to that reported for the hemisphere mass observable [22], which is $+1.363$. An explanation for this difference is provided in the latter reference. Similar observations were reported for the two-loop results for both CLs and NGLs.

C/A clustering reduces the k_t CLs coefficients by 45% at $R = 0$ to approximately 95% at $R = 1$. Additionally, unlike k_t, the magnitude of the C/A CLs coefficients decreases with increasing R (red curve). Since CLs are notoriously difficult to compute even at the first few
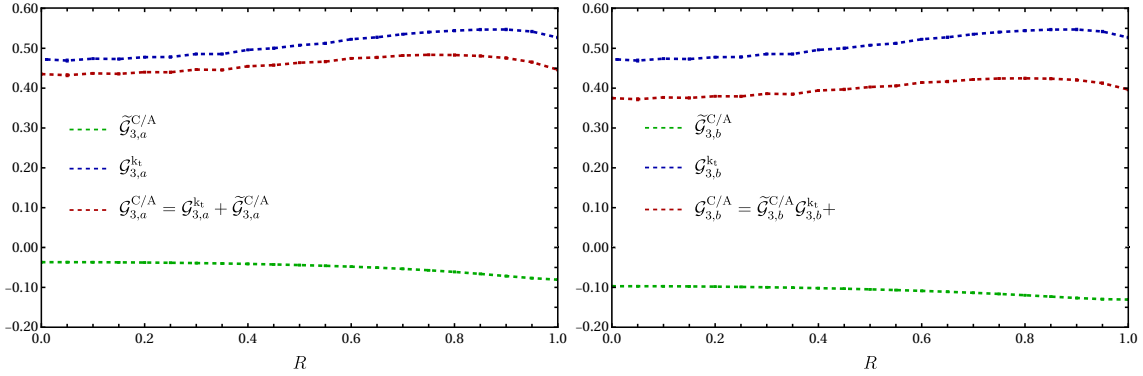
Figure 3: The three-loop NGLs coefficients for the C/A and k_t jet algorithms.

orders of perturbative expansion and at leading logarithmic accuracy, minimising their impact—or removing them entirely—would be highly desirable. These two features make the C/A algorithm preferable to k_t (at least at this loop order). Indeed, at $R = 1$:

$$\Sigma_{3,\text{cl}}^{\text{C/A}}(\rho) = +\bar{\alpha}_s^3 L^3 (0.0033), \qquad \Sigma_{3,\text{cl}}^{k_t}(\rho) = +\bar{\alpha}_s^3 L^3 (0.058). \qquad (19)$$

Comparing this to the leading term $\bar{\alpha}_s^3 L^6 (0.39)$, the CLs contribution is negligible, accounting for less than 0.8% of the leading term (compared to approximately 15% for k_t CLs).

In Fig. 3, we plot the results of the integrals in Eqs. (18) alongside the corresponding k_t results from Ref. [31]. The sums $\mathcal{G}_{3,i}^{\text{C/A}} = \widetilde{\mathcal{G}}_{3,i}^{\text{C/A}} + \mathcal{G}_{3,i}^{k_t}$ (where $i = a, b$), representing the total C/A NGLs coefficients at this loop order, are also plotted.

The C/A corrections to the k_t results are relatively small. However, similar to the CLs case, these corrections have the opposite sign to the k_t coefficients, thus reducing the final C/A NGLs coefficients. The reduction ranges from approximately 8% at $R = 0$ to 18% at $R = 1$ for the $C_F^2 C_A$ coefficient ($\mathcal{G}_{3,a}$), and from 26% at $R = 0$ to 33% at $R = 1$ for the $C_F C_A^2$ coefficient ($\mathcal{G}_{3,b}$). Similar to CLs, the magnitude of NGLs is smaller in C/A than in k_t clustering. Given the extreme complexity of calculating both CLs and NGLs, this makes C/A preferable to k_t, as an ideal jet algorithm should minimise the impact of non-global effects (whether CLs or NGLs).

In the small-R limit, we obtain $\mathcal{G}_{3,a}^{\text{C/A}}(0) = +0.37$ and $\mathcal{G}_{3,b}^{\text{C/A}}(0) = +0.57$. These values differ from their hemisphere mass counterparts [22]: $\mathcal{G}_{3,a}^{\text{C/A,hemi}} = +0.655$ and $\mathcal{G}_{3,b}^{\text{C/A,hemi}} = +0.198$. This discrepancy may be due to differences in the geometric distortion of the jet boundary across algorithms, as explained in the latter reference. Since CLs and NGLs manifestly originate from the jet boundary, its geometric shape plays a crucial role in determining their magnitude.

To assess the impact of the C/A and k_t algorithms on the jet mass distribution, we compare them to the anti-k_t algorithm, which is free of CLs but exhibits relatively large NGLs. This comparison is shown in Fig. 4, where we sum both CLs and NGLs contributions (Eqs. (15) and (16)) including colour factors. The anti-k_t and k_t results are taken from our previous paper [31]. The reduction in the anti-k_t NGLs coefficient varies slightly for both k_t and C/A over the jet radii considered. For k_t, it ranges from 42% ($R = 0$) to 40% ($R = 1$), while for C/A it increases from 52% ($R = 0$) to 54% ($R = 1$). The C/A clustering algorithm reduces the total non-global contribution to the jet mass distribution by more than 50% compared to anti-k_t, making it preferable to both anti-k_t and k_t for mitigating non-global effects at three loops.

In the next section, we present calculations of the four-loop CLs and NGLs coefficients for the jet mass observable. Together with the three-loop NGLs, these represent the state-of-the-art in fixed-order C/A clustering calculations and, to the best of our knowledge, have not been previously reported in the literature.
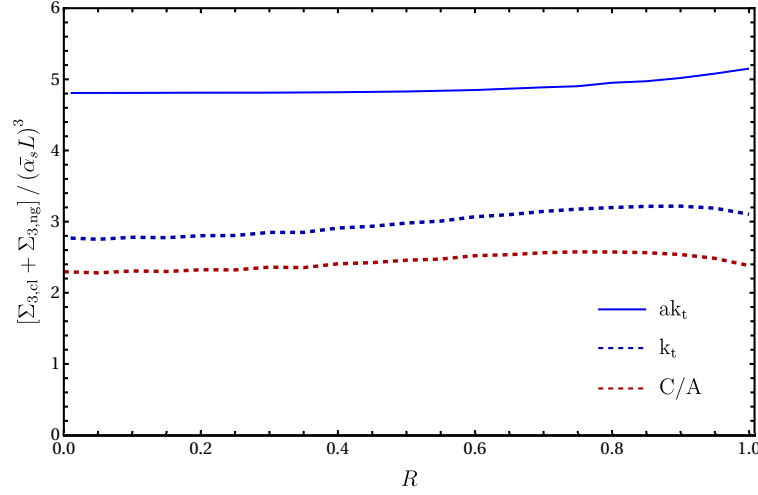
Figure 4: The sum of CLs and NGLs contributions to the jet mass fraction at three loops for three jet algorithms.

Δ_{12q}	Δ_{13q}	Δ_{14q}	Δ_{23q}	Δ_{24q}	Δ_{34q}	Orderings	4_{in}	$(3,4)_{\text{in}}$	$(2,4)_{\text{in}}$	$(1,4)_{\text{in}}$
0	0	0	0	1	1	$d_{24} < d_{34}$	C	C	C	C
0	0	0	0	1	1	$d_{34} < d_{24}$	C	C	C	C
0	0	0	1	1	1	$d_{23} < d_{24} < d_{34}$	C	C	C	C
0	0	0	1	1	1	$d_{23} < d_{34} < d_{24}$	C	C	C	C
0	0	0	1	1	1	$d_{24} < d_{23} < d_{34}$	C	C	C	C
0	0	0	1	1	1	$d_{24} < d_{34} < d_{23}$	C	C	C	C
0	0	0	1	1	1	$d_{34} < d_{23} < d_{24}$	C	C	C	C
0	0	0	1	1	1	$d_{34} < d_{24} < d_{23}$	C	C	C	C

Table 4: A sample of C/A algorithm results at four loops.

3.2 Four loops

For the emission of four soft, energy-ordered gluons, applying the C/A algorithm becomes considerably more complex, yielding lengthy and intricate expressions. To manage this complexity, we automated the entire process using a `Python` code. This code generates a comprehensive table containing all possible configurations, their corresponding orderings, and the resulting expressions for the sum of eikonal amplitudes that contribute to the mis-cancellation between real emissions and virtual corrections. The code is readily generalisable to higher loop orders. In total, there are $2^6 = 64$ possible configurations with 1957 distinct orderings.

Table 4 presents a sample of the code output (with explicit eikonal amplitude expressions replaced by 0 or C, as in the three-loop case). We show only the gluonic scenarios that exhibit mis-cancellations. The remaining scenarios not explicitly shown are: $(1,2,4)_{\text{in}}$, $(1,3,4)_{\text{in}}$, $(2,3,4)_{\text{in}}$, and $(1,2,3,4)_{\text{in}}$. Scenarios free of such mis-cancellations—and thus yielding no large logarithms—include cases such as 1_{in}, 2_{in}, 3_{in}, $(1,2)_{\text{in}}$, and several others.

To illustrate the C/A algorithm at four loops, consider the third row of Table 4 for case 4_{in} and ordering $d_{23} < d_{24} < d_{34}$. The 16 gluon configurations (RRRR, RRRV, RRVR, RVRR, etc.) yield the following clustering outcomes:

1. **RRRR**: Gluons 2 and 3 merge first into a subjet aligned with gluon 2 (due to strong ordering). Gluon 4 is then pulled out of the jet and merged with gluon 2, forming a subjet again aligned with gluon 2. The final configuration (gluons 1 and 2 outside the
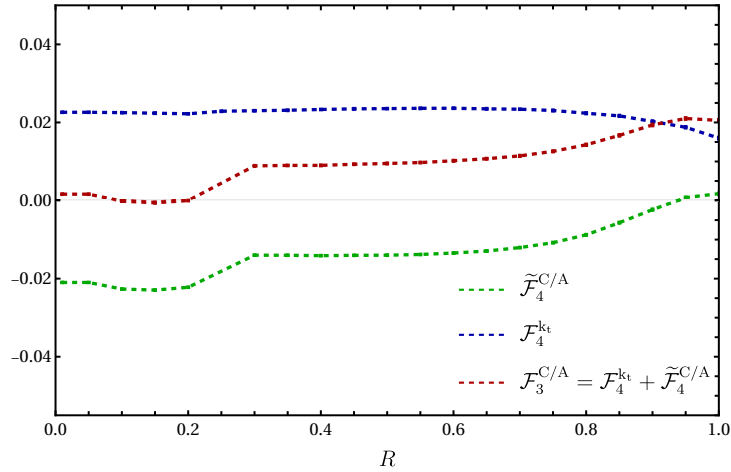
Figure 5: The four-loop CLs coefficient for the C/A and k_t jet algorithms.

jet) yields no jet mass contribution. The RRRV configuration has identical but opposite eikonal amplitude and cancels with RRRR.

2. **RRVR**: Gluon 3 is virtual and unaffected. Gluons 2 and 4 merge into a subjet aligned with gluon 2, leaving gluons 1 and 2 outside the jet—no mass contribution. This cancels with RRVV.

3. **RVRR**: Gluon 3 pulls gluon 4 out of the jet, forming a subjet aligned with gluon 3. Gluons 1 and 3 remain outside the jet—no mass contribution. This cancels with RVRV.

4. **VRRR**: Identical to RRRR, with no mass contribution. Cancels with VRRV.

5. **VVRR**: Gluon 3 pulls gluon 4 out of the jet—no mass contribution. Cancels with VVRV.

6. **VRVR**: Gluon 2 pulls gluon 4 out of the jet—no mass contribution. Cancels with VRVV.

7. **RVVR**: Gluons 2 and 3 are virtual and cannot affect gluon 4, which remains inside the jet and contributes to its mass. The counterpart RVVV has no contribution (gluon 4 virtual), resulting in a real–virtual mis-cancellation.

8. **VVVR**: Identical to RVVR, contributing to the jet mass. Not cancelled by VVVV (gluon 4 virtual).

The final expression for this case (third row, 4_in) is:

$$-\Theta_1^\text{out}\Theta_2^\text{out}\Theta_3^\text{out}\Theta_4^\text{in}\,\Theta_4^\rho\,\Theta\left(d_{34}-d_{24}\right)\Theta\left(d_{24}-d_{23}\right)\left[\mathcal{W}_{1234}^\text{RVVR}+\mathcal{W}_{1234}^\text{VVVR}\right]. \tag{20}$$

This calculation is repeated for all 1957 cases. For each configuration, we sum contributions from all orderings, yielding 64 total expressions. These tasks are performed by the `Python` code. Using `Mathematica` and the full k_t contribution from [31], we subtract the k_t component to isolate new C/A clustering contributions. We substitute explicit eikonal amplitude expressions from ref. [38], split coefficients by colour factor, and compute them numerically using the `Cuba` library [42].

The jet mass fraction at four loops takes a form analogous to the three-loop case (14):

$$\begin{aligned}
\Sigma_4^\text{C/A}(\rho) &= \Sigma_4^{k_t} + \widetilde{\Sigma}_4^\text{C/A}, \\
&= \frac{1}{4!}\left(\Sigma_1\right)^4 + \Sigma_1 \times \left(\Sigma_{3,\text{cl}}^\text{C/A}+\Sigma_{3,\text{ng}}^\text{C/A}\right) + \frac{1}{2!}\left(\Sigma_1\right)^2 \times \left(\Sigma_{2,\text{cl}}^\text{C/A}+\Sigma_{2,\text{ng}}^\text{C/A}\right) + \frac{1}{2!}\left(\Sigma_{2,\text{cl}}^\text{C/A}\right)^2 \\
&\quad + \frac{1}{2!}\left(\Sigma_{2,\text{ng}}^\text{C/A}\right)^2 + \Sigma_{4,\text{cl}}^\text{C/A} + \Sigma_{4,\text{ng}}^\text{C/A},
\end{aligned} \tag{21}$$
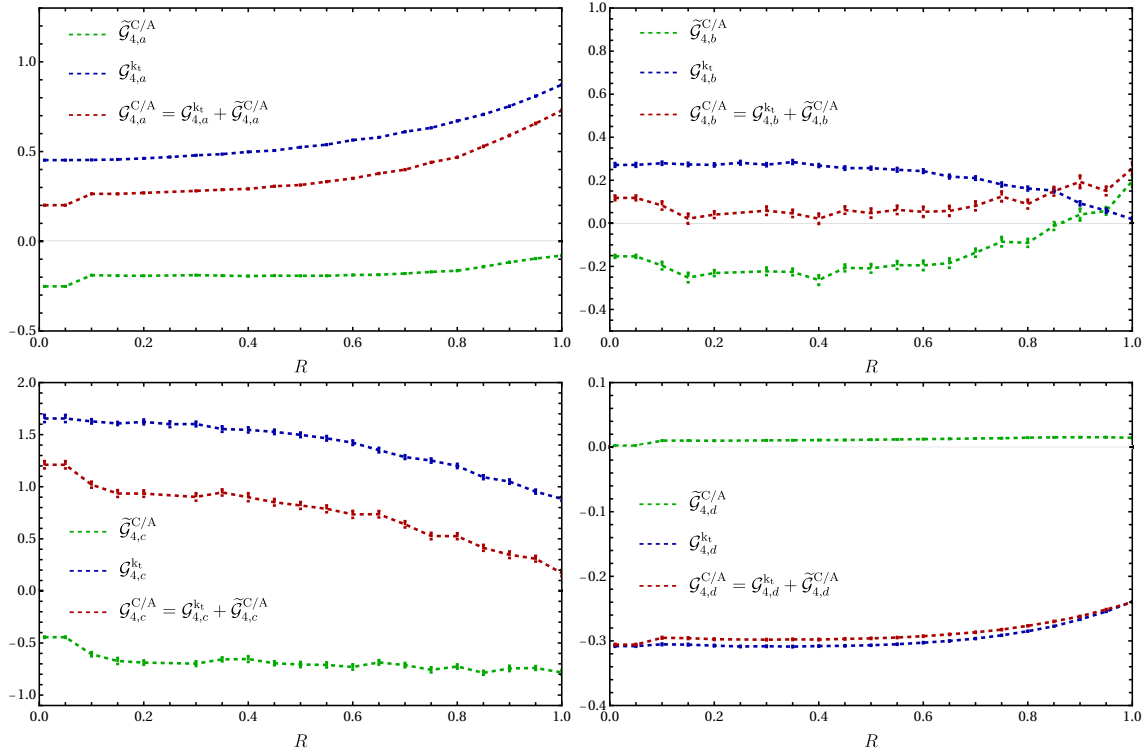
Figure 6: The four-loop NGLs coefficients for the C/A and k_t jet algorithms.

where the new C/A clustering contributions are (see Refs. [22, 31]):

$$\Sigma_{4,\text{cl}}^{\text{C/A}}(\rho) = +2\bar{\alpha}_s^4 \frac{L^4}{4!} C_F^4 \left[\mathcal{F}_4^{\text{k}_t} + \widetilde{\mathcal{F}}_4^{\text{C/A}} \right], \tag{22}$$

for the CLs contribution, and:

$$\Sigma_{4,\text{ng}}^{\text{C/A}}(\rho) = -2\bar{\alpha}_s^4 \frac{L^4}{4!} \Big[-C_F^3 C_A \left(\mathcal{G}_{4,a}^{\text{k}_t} + \widetilde{\mathcal{G}}_{4,a}^{\text{C/A}} \right) - C_F^2 C_A^2 \left(\mathcal{G}_{4,b}^{\text{k}_t} + \widetilde{\mathcal{G}}_{4,b}^{\text{C/A}} \right) + C_F C_A^3 \left(\mathcal{G}_{4,c}^{\text{k}_t} + \widetilde{\mathcal{G}}_{4,c}^{\text{C/A}} \right) + $$
$$ + C_F C_A^2 \left(C_A - 2C_F \right) \left(\mathcal{G}_{4,d}^{\text{k}_t} + \widetilde{\mathcal{G}}_{4,d}^{\text{C/A}} \right) \Big], \tag{23}$$

for the NGLs contribution.

Integration results as functions of the jet radius R are shown in Figs. 5 and 6. Apart from minor irregularities at very small R values (attributable to limited statistics[1]), C/A clustering induces substantial reductions in both CLs and NGLs coefficients across most R values. However, for $R \gtrsim 0.85$, the C/A coefficients—particularly $\mathcal{F}_4^{\text{C/A}}$ and $\mathcal{G}_{4,b}^{\text{C/A}}$—become comparable to or exceed their k_t counterparts.

These observations are confirmed in Fig. 7, which plots the combined CLs and NGLs contributions for C/A, k_t, and anti-k_t algorithms. In addition to the sign change of the C/A contribution (positive, unlike the negative contributions of k_t and anti-k_t), the reduction ranges from 92% at $R = 0$ to 74% at $R = 1$. For k_t, the reduction varies between 63% and 78% over the same range. At $R = 1$, the k_t reduction slightly exceeds that of C/A. Overall, we conclude that up to four loops at single-logarithmic accuracy, the C/A clustering algorithm should be prioritised over both anti-k_t and k_t for studies of non-global observables, as it minimises the impact of non-global logarithms (both CLs and NGLs).

---

[1]We employed approximately 10^{11} integrand evaluations for the `Vegas` routine in the `Cuba` library.
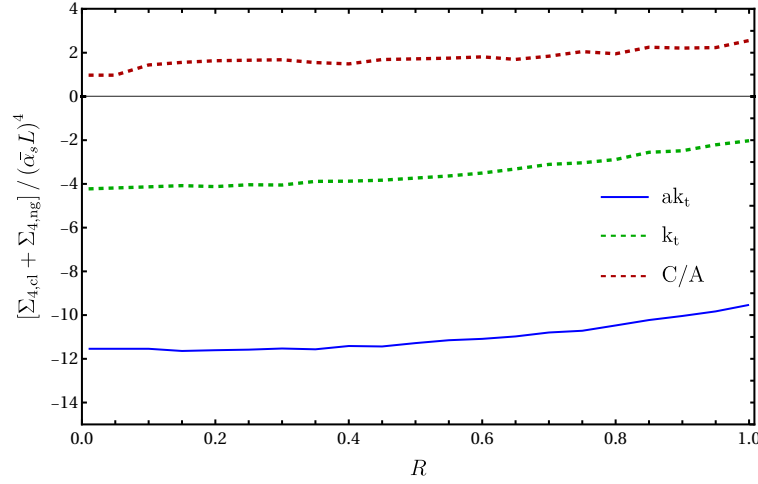
Figure 7: Comparison of combined CLs and NGLs effects at four loops for three jet algorithms.

Comparing with our previous hemisphere mass calculations [22], the small-R limit values:

$$\mathcal{F}_4^{\text{C/A}} = 0.02, \quad \mathcal{G}_{4,a}^{\text{C/A}} = 0.2, \quad \mathcal{G}_{4,b}^{\text{C/A}} = 0.12, \quad \mathcal{G}_{4,c}^{\text{C/A}} = 1.21, \quad \mathcal{G}_{4,d}^{\text{C/A}} = -0.31, \tag{24}$$

differ significantly from those in eqs. (49) and (52) of [22]. This discrepancy may stem from geometric distortion of the jet boundary, as discussed previously.

In the next section, we discuss the exponentiation of CLs and NGLs for the C/A algorithm and compare their impacts on the full resummed jet mass distribution with those of anti-k_t and k_t.

4 All-order treatment

Since the C/A algorithm encompasses the k_t algorithm, as explained in previous sections, it follows an identical structure and introduces only additional corrections absent in the latter. Therefore, the exponentiation of both CLs and NGLs reported in previous studies (see, for instance, [1, 22, 30, 31, 37]) for anti-k_t and k_t algorithms also holds for C/A clustering. Accordingly, we write the full resummed jet mass distribution up to NLL accuracy in the standard form [1, 6, 22, 31, 36]:

$$\Sigma^{\text{C/A}}(\rho) = \Sigma^{\text{p}}(\rho) \mathcal{S}^{\text{C/A}}(\rho) \mathcal{C}^{\text{C/A}}(\rho), \tag{25}$$

where $\Sigma^{\text{p}}(\rho)$ is the familiar Sudakov form factor that resums leading double logarithms from soft and collinear emissions, given by [43]:

$$\Sigma^{\text{p}}(\rho) = \frac{\exp\left[-\mathcal{R} - \gamma_E \mathcal{R}'\right]}{\Gamma(1 + \mathcal{R}')}, \tag{26}$$

where the radiator $\mathcal{R}$ contains both leading and next-to-leading large logarithmic contributions to the jet mass fraction, $\mathcal{R}'$ is its derivative with respect to $\tilde{L} = \ln(R^2/\rho)$, and $\gamma_E = 0.577$ is the Euler–Mascheroni constant. Note that at single-logarithmic accuracy, $\tilde{L} \sim L = \ln(1/\rho)$. The full expressions for $\mathcal{R}$ and its derivative can be found in, for instance, Refs. [4, 6, 22].

The NGLs form factor for C/A clustering, $\mathcal{S}^{\text{C/A}}(\rho)$, resums the leading single-logarithmic NGLs to all orders. Unfortunately, there exists neither an analytical formula nor a numerical estimate of its size. The Monte Carlo code of Ref. [1] does not implement the C/A jet algorithm,

though it can compute NGLs resummed form factor for soft and collinear observables such as the jet mass. Other numerical resummation approaches, such as [9, 10, 18], either lack the C/A jet algorithm or are only valid for soft large-angle observables like gaps-between-jets. We thus resort to estimating it using the fixed-order calculations up to four loops presented in previous sections, and the observed exponentiation pattern. Accordingly, we write, following analogous calculations for anti-k_t and k_t algorithms [22, 23, 31, 36]:

$$\mathcal{S}^{\text{C/A}}(t) = \exp\left[-2\sum_{n\geq 2}\frac{1}{n!}\mathcal{S}_n^{\text{C/A}}(R)(-2\,t)^n\right], \tag{27}$$

where the n-loop NGLs coefficients are given, up to four loops, by:

$$\mathcal{S}_2^{\text{C/A}} = C_F C_A \, \mathcal{G}_2^{\text{C/A}}, \quad \mathcal{S}_3^{\text{C/A}} = C_F^2 C_A \, \mathcal{G}_{3,a}^{\text{C/A}} + C_F C_A^2 \, \mathcal{G}_{3,b}^{\text{C/A}},$$
$$\mathcal{S}_4^{\text{C/A}} = -C_F^3 C_A \, \mathcal{G}_{4,a}^{\text{C/A}} - C_F^2 C_A^2 \, \mathcal{G}_{4,b}^{\text{C/A}} + C_F C_A^3 \, \mathcal{G}_{4,c}^{\text{C/A}} + C_F^2 \left(C_A - 2C_F\right) \mathcal{G}_{4,d}^{\text{C/A}}. \tag{28}$$

Here t is the evolution variable, which at single-logarithmic accuracy is given by [1, 4, 31]:

$$t = \frac{1}{2\pi}\int_{\rho/R^2}^{1}\frac{\mathrm{d}x}{x}\,\alpha_s\,(xQ/2) = -\frac{1}{4\pi\beta_0}\ln\left[1 - 2\alpha_s\beta_0\tilde{L}\right], \tag{29}$$

where $\alpha_s \equiv \alpha_s(QR/2)$ and the last equality shows the one-loop expansion of the integral, sufficient for our NLL accuracy. Note that for a fixed coupling, $t = \bar{\alpha}_s\tilde{L}/2$. Furthermore, expanding (27) yields the NGLs contributions at two, three, and four loops (Eqs. (12d), (16), and (23), respectively).

The CLs form factor for the C/A algorithm, $\mathcal{C}^{\text{C/A}}(\rho)$, resums the leading single-logarithmic clustering logarithms for the jet mass observable. Similar to the NGLs form factor, there exists neither an analytical formula nor a numerical estimate for it. Since it also exhibits an exponentiation pattern, we can express it as an exponential of the fixed-order results. To this end, we write it in a form analogous to that for NGLs (27):

$$\mathcal{C}^{\text{C/A}}(t) = \exp\left[2\sum_{n\geq 2}\frac{1}{n!}\mathcal{F}_n^{\text{C/A}}(R)(-2\,C_F\,t)^n\right], \tag{30}$$

where the CLs coefficients at two, three, and four loops are given in Eqs. (12c), (15), and (22), respectively.

As stated above, there are no all-orders results for the jet mass observable—either numerical or analytical—in either the finite-N_c or large-N_c limits. To quantify the impact of the NGLs and CLs exponentials (27) and (30), we compare them to the output of the MC code [1] for the anti-k_t and k_t algorithms. For this purpose, we use the well-known parametrisations (see, for instance, Refs. [1, 6, 23, 24]):

$$\mathcal{S}_{\text{MC}}(t) = \exp\left[-C_F C_A \, \mathcal{G}_2(R)\left(\frac{1 + (at)^2}{1 + (bt)^c}\right)t^2\right], \tag{31}$$

for the NGLs form factor, and

$$\mathcal{C}_{\text{MC}}(\rho) = \exp\left[C_F^2 \, \mathcal{F}_2(R)\left(\frac{1 + (at)^2}{1 + (bt)^c}\right)t^2\right], \tag{32}$$

for the CLs form factor. The values of the two-loop coefficients $\mathcal{G}_2(R)$ and $\mathcal{F}_2(R)$, along with the fitting parameters a, b, and c, are presented in Tables 1 and 2 of Ref. [31] for $R = 0.7$ and 1.0.
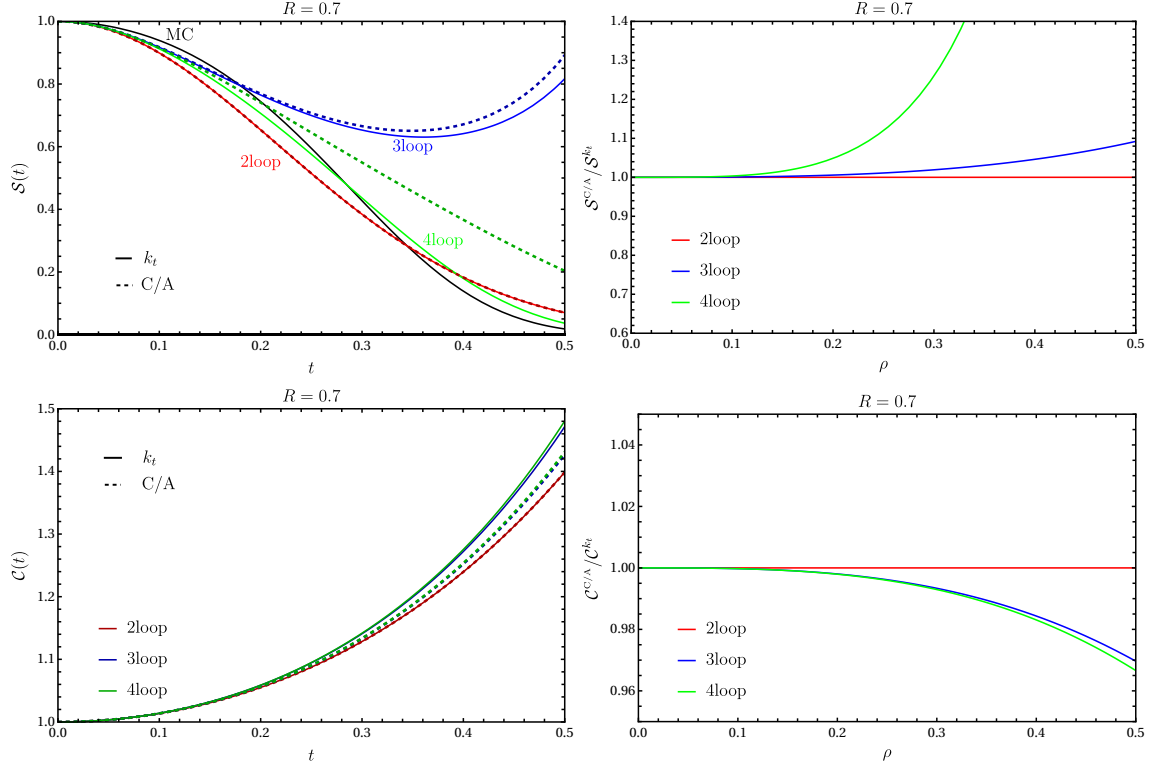
Figure 8: Comparison of the exponentials $\mathcal{S}(t)$ (Eq. (27)) and $\mathcal{C}(t)$ (Eq. (30)) for k_t and C/A jet algorithms with $R = 0.7$. Solid lines: k_t; dashed lines: C/A. The black line shows the Monte Carlo output for the k_t algorithm.

In Fig. 8, we plot the NGLs and CLs exponentials (Eqs. (27) and (30)) for k_t (solid lines) and C/A (dashed lines) algorithms with jet radius $R = 0.7$. The two-loop results are identical, as mentioned in Sec. 3, hence the curves coincide. The three- and four-loop C/A curves for $\mathcal{S}(t)$ are slightly higher than those for k_t, indicating a reduction in the corresponding fixed-order NGLs coefficients, as observed previously (recall the NGLs exponent is negative). This is clearly visible in the right-hand side plots, which show the ratio of C/A to k_t form factors. Note that the calculations are more reliable for smaller t [36], and including more higher-loop coefficients extends the range of t over which the results are reliable. For CLs, since the exponent is positive, smaller terms yield a smaller exponent. We observe that the C/A curves are slightly lower than those for k_t, again indicating that their corresponding fixed-order coefficients are smaller in magnitude. This is clearly supported by the ratio plot. Note that for $\mathcal{C}(t)$, the difference between the three- and four-loop results is minuscule for both k_t and C/A, largely due to the small coefficient sizes and the $1/n!$ prefactor.

In Fig. 9, we plot the full NLL-resummed form factor (25) for three jet algorithms. For the anti-k_t and k_t algorithms, we use the MC parametrisations (31) and (32) for the NGLs and CLs form factors, respectively, while for C/A clustering we use the exponentials (27) and (30). The left-hand side plots compare the full form factor where the C/A NGLs and CLs exponentials include terms up to two, three, and four loops, for $R = 0.7$ and $R = 1.0$. The two-loop curves exhibit a shift in the Sudakov peak position and a reduction in its height of about 10% for $R = 0.7$ and 8% for $R = 1.0$. The three- and four-loop curves are nearly identical, again featuring a peak shift and height reduction of about 8% for $R = 0.7$ and 6% for $R = 1.0$.

The four-loop C/A results are plotted alongside the corresponding four-loop k_t results, MC outputs for anti-k_t and k_t, and the Sudakov form factor in the right-hand side plots of Fig. 9 for both R values. The anti-k_t curve exhibits the largest peak shift and Sudakov peak height
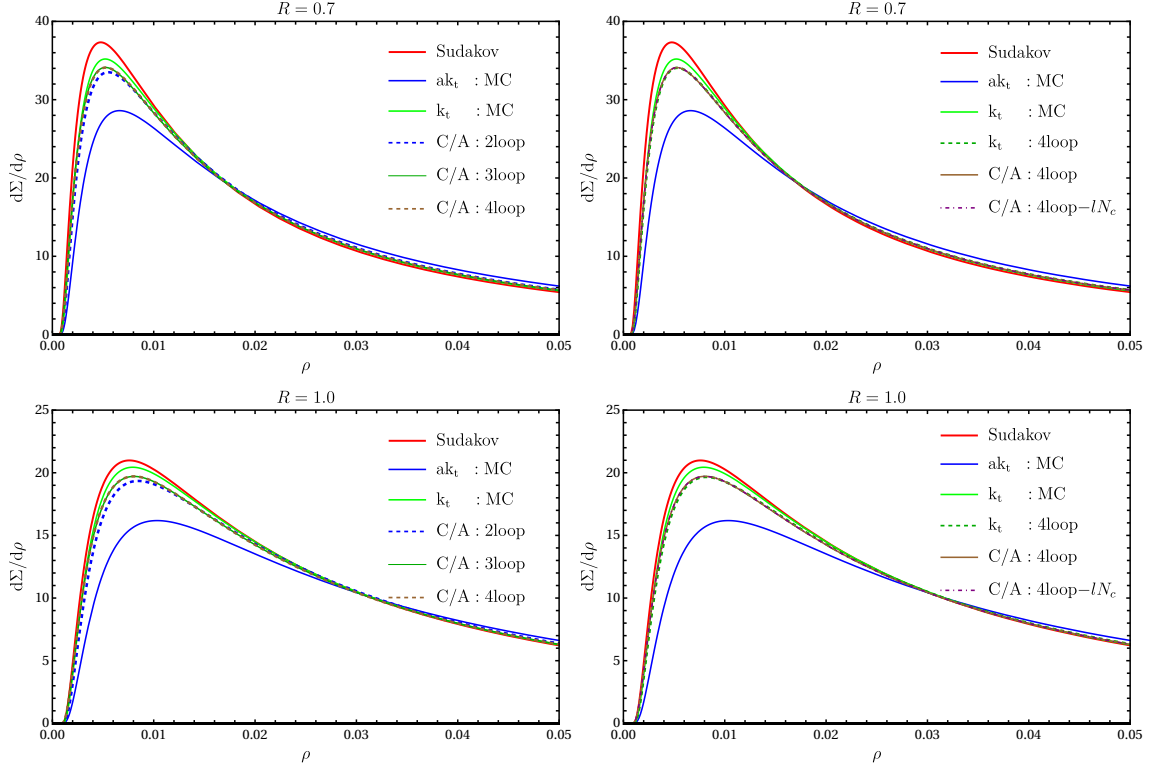
Figure 9: The full NLL-resummed form factor of the jet mass observable for anti-k_t, k_t, and C/A jet algorithms with $R = 0.7$ and $R = 1.0$. The notation "lN_c" denotes the large-N_c limit.

reduction, reaching up to 23%. This is followed by the four-loop curves for both k_t and C/A, with the C/A distribution slightly lower than that of k_t, showing reductions of up to 8% and 6% for $R = 0.7$ and $R = 1.0$, respectively. The all-orders MC result for k_t performs best, with Sudakov peak height reductions of only about 6% and 3% for the two R values, respectively. Since the C/A four-loop distribution performs slightly better than the corresponding k_t distribution in minimising the overall impact of NGLs and CLs, we expect the all-orders result to perform better than that of k_t.

It is worth noting that switching off the finite-N_c corrections by setting $C_A = 2C_F$ in the four-loop NGLs coefficient for the C/A algorithm has no noticeable effect on the curves in Fig. 9. This corresponds to the large-N_c approximation, denoted by "lN_c" in the plots.

5 Conclusion

In this paper, we have computed, for the first time in the literature, the full fixed-order distribution of a QCD non-global observable up to four loops at single-logarithmic accuracy in e^+e^- annihilation to dijets, where jets are defined using the Cambridge-Aachen sequential recombination algorithm. We have explicitly demonstrated that the structure of the C/A algorithm is considerably more complex, and the associated analytical calculations substantially more involved, than for its counterparts, the anti-k_t and k_t algorithms. The primary source of complexity stems from the fact that C/A involves no intrinsic ordering parameter. In other words, the distance between any pair of final-state particles is equally likely to be the smallest, in contrast to k_t, where clustering distances are weighted by the square of the particles' transverse momenta.

We have shown that while C/A is identical to k_t at two loops, the algorithms begin to differ at higher orders. We have therefore presented detailed calculations of the full jet mass distribution at three and four loops at the single-logarithmic level (terms of the form $\alpha_s^n L^n$). These involve computing both CLs and NGLs contributions, which are particularly delicate to determine given the aforementioned complexity of the C/A algorithm for analytical calculations. In general, the C/A algorithm encompasses k_t, in the sense that the full contribution of the latter is contained within the former. Additionally, C/A introduces new corrections beyond the scope of the k_t algorithm. These corrections are generally of opposite sign to the k_t contributions for both NGLs and CLs, thereby reducing the overall impact of non-global logarithms to varying degrees.

The all-orders treatment of the NGLs and CLs contributions for the C/A algorithm was limited to comparisons with results from the anti-k_t and k_t algorithms, primarily due to the absence of all-orders analytical or numerical evaluations for C/A clustering. Overall, within the approximations and accuracy of this work, the C/A algorithm performs better than the other two in minimising the effect of non-global logarithms. Since non-global effects are notoriously difficult to compute—both at fixed order and to all orders, even at leading logarithmic accuracy—finding ways to mitigate them is highly desirable. The C/A algorithm appears to be a promising candidate for achieving this goal. Whether higher-loop calculations and/or all-orders resummation of C/A logarithms confirm this observation remains to be seen and will be the subject of future work.

It would be worthwhile to apply the current techniques and results to more complex QCD environments, exploring how the C/A algorithm compares to other jet algorithms in such multi-scale processes. Developing an integro-differential equation similar to that of Banfi, Marchesini, and Smye, or a computational code analogous to that of Dasgupta and Salam that incorporates C/A clustering, would constitute a major step toward a deeper and more insightful understanding of how complex jet algorithms reshape the impact of non-global logarithms.

References

[1] M. Dasgupta and G. P. Salam, *Resummation of nonglobal QCD observables*, Phys. Lett. B **512**, 323 (2001), doi:10.1016/S0370-2693(01)00725-0, hep-ph/0104277.

[2] A. Banfi, G. Marchesini and G. Smye, *Away from jet energy flow*, JHEP **08**, 006 (2002), doi:10.1088/1126-6708/2002/08/006, hep-ph/0206076.

[3] R. B. Appleby and M. H. Seymour, *Nonglobal logarithms in interjet energy flow with k_t clustering requirement*, JHEP **12**, 063 (2002), doi:10.1088/1126-6708/2002/12/063, hep-ph/0211426.

[4] A. Banfi, M. Dasgupta, K. Khelifa-Kerfa and S. Marzani, *Non-global logarithms and jet algorithms in high-pT jet shapes*, JHEP **08**, 064 (2010), doi:10.1007/JHEP08(2010)064, 1004.3483.

[5] A. Banfi and M. Dasgupta, *Problems in resumming interjet energy flows with k(t) clustering*, Phys. Lett. **B628**, 49 (2005), doi:10.1016/j.physletb.2005.08.125, hep-ph/0508159.

[6] K. Khelifa-Kerfa, *QCD resummation for high-p_T jet shapes at hadron colliders*, Ph.D. thesis, Manchester U. (2012), 2111.10671.

[7] M. Cacciari, G. P. Salam and G. Soyez, *The anti-k_t jet clustering algorithm*, JHEP **04**, 063 (2008), doi:10.1088/1126-6708/2008/04/063, 0802.1189.

[8] H. Weigert, *Nonglobal jet evolution at finite N(c)*, Nucl. Phys. B **685**, 321 (2004), doi:10.1016/j.nuclphysb.2004.03.002, hep-ph/0312050.

[9] Y. Hatta and T. Ueda, *Resummation of non-global logarithms at finite N_c*, Nucl. Phys. B **874**, 808 (2013), doi:10.1016/j.nuclphysb.2013.06.021, 1304.6930.

[10] Y. Hagiwara, Y. Hatta and T. Ueda, *Hemisphere jet mass distribution at finite N_c*, Phys. Lett. B **756**, 254 (2016), doi:10.1016/j.physletb.2016.03.028, 1507.07641.

[11] Y. Hatta and T. Ueda, *Non-global logarithms in hadron collisions at $N_c = 3$*, Nucl. Phys. B **962**, 115273 (2021), doi:10.1016/j.nuclphysb.2020.115273, 2011.04154.

[12] A. Banfi, F. A. Dreyer and P. F. Monni, *Next-to-leading non-global logarithms in QCD*, JHEP **10**, 006 (2021), doi:10.1007/JHEP10(2021)006, 2104.06416.

[13] A. Banfi, F. A. Dreyer and P. F. Monni, *Higher-order non-global logarithms from jet calculus*, JHEP **03**, 135 (2022), doi:10.1007/JHEP03(2022)135, 2111.02413.

[14] T. Becher, N. Schalch and X. Xu, *Resummation of Next-to-Leading Nonglobal Logarithms at the LHC*, Phys. Rev. Lett. **132**(8), 081602 (2024), doi:10.1103/PhysRevLett.132.081602, 2307.02283.

[15] S. Ferrario Ravasio, K. Hamilton, A. Karlberg, G. P. Salam, L. Scyboz and G. Soyez, *Parton Showering with Higher Logarithmic Accuracy for Soft Emissions*, Phys. Rev. Lett. **131**(16), 161906 (2023), doi:10.1103/PhysRevLett.131.161906, 2307.11142.

[16] S. Catani, Y. L. Dokshitzer, M. H. Seymour and B. R. Webber, *Longitudinally invariant K_t clustering algorithms for hadron hadron collisions*, Nucl. Phys. B **406**, 187 (1993), doi:10.1016/0550-3213(93)90166-M.

[17] S. D. Ellis and D. E. Soper, *Successive combination jet algorithm for hadron collisions*, Phys. Rev. **D48**, 3160 (1993), doi:10.1103/PhysRevD.48.3160, hep-ph/9305266.

[18] T. Becher and J. Haag, *Factorization and resummation for sequential recombination jet cross sections*, JHEP **01**, 155 (2024), doi:10.1007/JHEP01(2024)155, 2309.17355.

[19] Y. L. Dokshitzer, G. D. Leder, S. Moretti and B. R. Webber, *Better jet clustering algorithms*, JHEP **08**, 001 (1997), doi:10.1088/1126-6708/1997/08/001, hep-ph/9707323.

[20] M. Wobisch and T. Wengler, *Hadronization corrections to jet cross-sections in deep inelastic scattering*, In *Workshop on Monte Carlo Generators for HERA Physics (Plenary Starting Meeting)*, pp. 270–279 (1998), hep-ph/9907280.

[21] Y. Delenda and K. Khelifa-Kerfa, *On the resummation of clustering logarithms for non-global observables*, JHEP **09**, 109 (2012), doi:10.1007/JHEP09(2012)109, 1207.4528.

[22] K. Khelifa-Kerfa and M. Benghanem, *Hemisphere mass up to four-loops with generalised k_t algorithms* (2025), 2506.14415.

[23] Y. Delenda, R. Appleby, M. Dasgupta and A. Banfi, *On QCD resummation with k(t) clustering*, JHEP **0612**, 044 (2006), doi:10.1088/1126-6708/2006/12/044, hep-ph/0610242.

[24] K. Khelifa-Kerfa, *Non-global logs and clustering impact on jet mass with a jet veto distribution*, JHEP **02**, 072 (2012), doi:10.1007/JHEP02(2012)072, 1111.2016.

[25] M. Dasgupta, K. Khelifa-Kerfa, S. Marzani and M. Spannowsky, *On jet mass distributions in Z+jet and dijet processes at the LHC*, JHEP **10**, 126 (2012), doi:10.1007/JHEP10(2012)126, 1207.1640.

[26] N. Ziani, K. Khelifa-Kerfa and Y. Delenda, *Jet mass distribution in Higgs/vector boson + jet events at hadron colliders with k_t clustering*, Eur. Phys. J. C **81**, 570 (2021), doi:10.1140/epjc/s10052-021-09379-z, 2104.11060.

[27] H. Benslama, Y. Delenda and K. Khelifa-Kerfa, *Dijet azimuthal decorrelation in e+e− annihilation*, Phys. Lett. B **840**, 137903 (2023), doi:10.1016/j.physletb.2023.137903, 2301.00860.

[28] K. Khelifa-Kerfa, *Non-global logarithms up to four loops at finite-N_c for V/H+jet processes at hadron colliders*, JHEP **10**, 079 (2024), doi:10.1007/JHEP10(2024)079, 2406.13753.

[29] H. Bouaziz, Y. Delenda and K. Khelifa-Kerfa, *Azimuthal decorrelation between a jet and a Z boson at hadron colliders*, JHEP **10**, 006 (2022), doi:10.1007/JHEP10(2022)006, 2207.10147.

[30] K. Khelifa-Kerfa and M. Benghanem, *Jet-mass in V/H+jet up to four-loops with k_t clustering* (2025), 2508.02462.

[31] K. Khelifa-Kerfa, *Dijet mass up to four loops with(out) k_t clustering*, Eur. Phys. J. C **85**(2), 133 (2025), doi:10.1140/epjc/s10052-025-13837-3, 2411.03956.

[32] K. Khelifa-Kerfa, *Clustering logarithms up to six loops*, Phys. Rev. D **111**(9), 094018 (2025), doi:10.1103/PhysRevD.111.094018, 2412.03244.

[33] R. B. Appleby and M. H. Seymour, *The Resummation of interjet energy flow for gaps between jets processes at HERA*, JHEP **09**, 056 (2003), doi:10.1088/1126-6708/2003/09/056, hep-ph/0308086.

[34] M. Cacciari, G. P. Salam and G. Soyez, *FastJet User Manual*, Eur. Phys. J. C **72**, 1896 (2012), doi:10.1140/epjc/s10052-012-1896-2, 1111.6097.

[35] M. D. Schwartz and H. X. Zhu, *Nonglobal logarithms at three loops, four loops, five loops, and beyond*, Phys. Rev. D **90**(6), 065004 (2014), doi:10.1103/PhysRevD.90.065004, 1403.4949.

[36] K. Khelifa-Kerfa and Y. Delenda, *Non-global logarithms at finite N_c beyond leading order*, JHEP **03**, 094 (2015), doi:10.1007/JHEP03(2015)094, 1501.00475.

[37] K. Khelifa-Kerfa, *Analytical structure of k_t clustering to any order*, Phys. Rev. D **111**(1), 014027 (2025), doi:10.1103/PhysRevD.111.014027, 2409.14029.

[38] Y. Delenda and K. Khelifa-Kerfa, *Eikonal gluon bremsstrahlung at finite N_c beyond two loops*, Phys. Rev. D **93**(5), 054027 (2016), doi:10.1103/PhysRevD.93.054027, 1512.05401.

[39] H. Benslama, Y. Delenda, K. Khelifa-Kerfa and A. M. Ibrahim, *Eikonal Amplitudes and Nonglobal Logarithms from the BMS Equation*, Phys. Part. Nucl. Lett. **18**(1), 5 (2021), doi:10.1134/S1547477121010039, 2006.06738.

[40] K. Khelifa-Kerfa and Y. Delenda, *Eikonal amplitudes for three-hard legs processes at finite-N_c*, Phys. Lett. B **809**, 135768 (2020), doi:10.1016/j.physletb.2020.135768, 2006.08758.

[41] M. Dasgupta and G. P. Salam, *Accounting for coherence in interjet E(t) flow: A Case study,* JHEP **03**, 017 (2002), doi:10.1088/1126-6708/2002/03/017, hep-ph/0203009.

[42] T. Hahn, *CUBA: A Library for multidimensional numerical integration,* Comput. Phys. Commun. **168**, 78 (2005), doi:10.1016/j.cpc.2005.01.010, hep-ph/0404043.

[43] S. Catani, L. Trentadue, G. Turnock and B. R. Webber, *Resummation of large logarithms in e+ e- event shape distributions,* Nucl. Phys. **B407**, 3 (1993), doi:10.1016/0550-3213(93)90271-P.